*Biochimica et Biophysica Acta*, 1101 (1992) 23–32



BBABIO 43621

# Distance of P680 from the manganese complex in Photosystem II studied by time resolved EPR

Yoshio Kodera, Keizo Takura and Asako Kawamori

*Faculty of Science, Kwansei Gakuin University, Nishinomiya (Japan)*

(Received 11 February 1992)

Key words: Photosystem II; EPR; Transient EPR signal; Spin-lattice relaxation; P680; Tyrosine-D; Manganese cluster

The flash-induced transient EPR signal of $P680^+$ was observed in PS II membranes at temperatures between 77 and 220 K. Below 180 K, the half decay time, $t_{1/2}$, of $P680^+$ transient signal was about 2 ms and re-reduction of $P680^+$ has been ascribed to the back reaction with $Q_A$. Above 200 K, the decay rate increased with an activation energy of 15.6 kJ/mol. These results were coincident with previous optical data of $P680^+$. Spin-lattice relaxation rates, $1/T_1$, of $P680^+$ and $Tyr.D^+$ EPR signals, were determined by microwave power saturation experiments and by $T_2$ measurements using a pulsed EPR in the $S_1$ and $S_2$ states of oxygen-evolving complex (OEC) at 90 K. The ratio of distances of both radical species from the manganese cluster in OEC was derived from the difference of $T_1$ values in the $S_1$ and $S_2$ states. The result has shown that the distance from OEC to P680 was 0.91 times as far as that to Tyr.D. On the basis of the temperature-dependence of the half saturation power $P_{1/2}$ of $Tyr.D^+$ in the $S_1Q_AFe^{2+}$ and $S_2Q_AFe^{2+}$ states we estimated that the distance from Tyr.D to the Mn-cluster in OEC to be 24–27 Å. The distance from R680 to the manganese cluster was estimated to be 21–26 Å. The distance of Tyr.D from $Q_AFe^{2+}$ was supposed to be 26–33 Å, from $1/T_1$ values in $Q_AFe^{2+}$ and $Q_AFe^{2+}$ at 90 K.

## Introduction

Light energy induces oxidation of the reaction center P680 in the Photosystem II of higher plants. This reaction occurs within nanoseconds [1,2] and oxidized P680 ($P680^+$ cation radical) is reduced by Tyr.Z with a halftime of 20–250 ns in oxygen-evolving PS II [3–5]. Next $Tyr.Z^+$, an oxidized form of Tyr.Z, is reduced by oxidation of one of the four cyclic states of the OEC [6] with a halftime between 30 μs and 1.5 ms, in accordance with the kinetics of S state transition [7–10]. On the other hand, the photoexcited electron of P680 transfers to a primary quinone acceptor, $Q_A$, then to a secondary acceptor $Q_B$ and eventually to PS I. $P680^+$ reduction kinetics are altered from the nanosecond to the microsecond time scale by the elimination of the $O_2$ evolving capacity by treatments such as Tris-washing or incubation with $NH_2OH$ [3,11]. If a charge separation between P680 and $Q_A$ takes place in the oxidized state of Tyr.Z, $P680^+$ will be reduced by charge recombination with $Q_A^-$ with a halftime of 150 ± 50 μs for a main phase in three-phase kinetics [11–14]. All these phenomena occurred at a physiological temperature. With lowering temperature below 200 K, where the OEC becomes gradually inactive [15], a charge recombination between $P680^+$ and $Q_A^-$ occurs [16–18] and the halftime of $P680^+$ decay kinetics is 3.0 ms below 180 K [19,20]. The temperature-dependence of $P680^+$ kinetics was measured in chloroplasts with treatments inhibiting oxygen-evolving activity and the activation energy above 200 K was estimated to be 13.8–15.5 kJ/mol for the charge recombination [17]. Thus the characteristics of the primary electron donor in PS II, $P680^+$, has been studied mainly by means of absorption change. Though the $P680^+$ EPR signal has been studied by several workers [18,20–25], observation of the EPR signal is usually difficult, because another similar signal due to $Chl^+$ [26,27] may appear at the same magnetic field.

The $P680^+$ EPR signal was observed by Malkin and Bearden [18], after their previously reported EPR signal [26] had been proved to be due to another chloro-

Correspondence: A. Kawamori, Faculty of Science, Kwansei Gakuin University, Uegahara 1-1-155, Nishinomiya 662, Japan.

Abbreviations: $(Bchl)_2$, bacterial chlorophyll dimer; PS II, Photosystem II; P680, primary electron donor of PS II; $Q_AFe^{2+}$, primary quinone-iron electron acceptor of PS II; $Q_B$, the secondary quinone electron acceptor of PS II; Tyr.Z, a tyrosine electron donor in D1 subunit of PS II; Tyr.D, a tyrosine electron donor in D2 subunit of PS II; OEC, oxygen-evolving complex; Chl, chlorophyll; Mn-cluster, manganese cluster; Sig. $II_s$, EPR signal of tyrosine $D^+$.

phyll radical [27]. The report [18] showed that the halftime of the $P680^+$ transient signal was 5 ms and independent of temperature between 5 K and 77 K. Similarity between Tyr.Z$^+$ rise and $P680^+$ decay kinetics in Tris-washed PS II has been observed at several pH values [21] at a physiological temperature proving Tyr.Z is a direct electron donor to $P680^+$. Nugent et al. [22] observed both $P680^+$ and Chl$^+$ EPR signals in the D1/D2/Cyt-*b*-559 complex. In the presence of Tyr.Z$^+$ by inhibition of electron donation from OEC to Tyr.Z in PSII, Ghanotakis and Babcock [23] and Bock et al. [24] obtained an EPR signal ascribed to $P680^+$ which has a similar line shape to the signal of Chl$^+$ [18], and which decayed with a halftime of 200 $\mu$s or less at 273 K [24]. Hoganson and Babcock [25] have shown the width of the $P680^+$ EPR signal, measured by a time-resolved EPR, to be 0.79 mT in the absence of Tyr.Z$^+$. These results on $P680^+$ observation were summarized by Miller and Brudvig with other EPR signals observable in PS II [28]. The effect of the oxidized form of the secondary electron donor Tyr.Z on the $P680^+$ EPR line shape was studied by time-resolved EPR and the distance between these radical species has been estimated to be 10–15 Å from line broadening of $P680^+$ [25].

The crystal structure of the reaction center in the purple bacterium *Rhodopseudomonas viridis* has been extensively studied by X-ray analysis [29]. On the other hand, the structures of the reaction centers on the photosystems of higher plants have not yet been clarified, because of difficulty in crystallization of the reaction center. At present the relaxation properties measured by EPR seem to be a useful method to obtain structural information in photosystem II, though the method is indirect, based on a magnetic interaction between a radical and other paramagnetic species. Several workers tried to find the correlation time of the S states in OEC with maximum relaxation effect on the Tyr.D$^+$ radical by measuring its half-saturation power [30], or saturation recovery time [31], though their results were not coincident with each other. By measuring $T_1$ of Tyr.D$^+$ in the different S states of the OEC by a pulsed EPR method below 30 K, the separation between Tyr.D and the Mn-cluster in the OEC was derived to be 28–43 Å from a maximum relaxation rate in the $S_0$ state at about 20 K [32]. On the other hand, the distances from Tyr.D to outer and inner surfaces of PS II membranes were estimated by the EPR power saturation characteristics of Tyr.D$^+$ to be 26 and 27 Å, respectively [33]. Isogai et al. [34] showed these distances of 36 and 20 Å, respectively, showing a good coincidence between both results. Svensson et al. [35] predicted the three-dimensional structure around the electron donors Tyr.Z and Tyr.D on the oxidizing side of PS II by using computer modeling from data of the photosynthetic reaction center in a purple bacteria and predicted the distance between the centers of each tyrosine and the closest Mg ion in P680 to be about 14 Å.

In this paper, the lifetime of a flash-induced $P680^+$ was measured between 90 K and 220 K in the $S_1$ state of oxygen-evolving PS II membranes by time-resolved EPR. The line shape and the temperature dependence of the decay kinetics of the transient signal were examined by comparison with the kinetics of $P680^+$ measured by optical measurement at low temperature in order to confirm that the observed transient signal was due to $P680^+$. Most of the EPR signals were measured at temperatures above 273 K, except for the works by Malkin and Bearden [18] and by Nugent et al. [20,22]. We tried to observe the $P680^+$ EPR signal at 90 K, where the Chl$^+$ radical remained as a steady signal or decayed slowly, and could obtain its line shape from the part decaying with a halftime of about 2 ms ascribed to the back reaction with $Q_A^-$. Because the measurement of $T_1$ of $P680^+$ with pulsed EPR was quite difficult, the value of $T_1$ of $P680^+$, was derived from $P_{1/2}$ obtained from the microwave saturation characteristics of the $P680^+$ radical species, combined with $T_2$ measurement with the pulse method. On the basis of the dipolar interaction of $P680^+$ with the manganese ions in OEC the ratio of relaxation rate ($1/T_1$) of $P680^+$ to Tyr.D$^+$ was determined in the same states of donor and acceptor. The ratio of distances of P680 and Tyr.D to the manganese cluster was derived. Then the absolute value of $1/T_1$ of Tyr.D$^+$ was estimated from the temperature dependencies of the $P_{1/2}$ of Tyr.D$^+$ in $S_1Q_A^-Fe^{2+}$ and $S_2Q_A^-Fe^{2+}$ states, in order to find the maximum contribution from the Mn-cluster in the $S_2$ state. Though the method is same as Evelo et al. [32], the redox state $S_2$ is different from their $S_0$, and may be more reliable. From these results we could estimate the absolute distance between P680 and the Mn-cluster of OEC.

## Materials and Methods

*Samples*

Oxygen-evolving PS II membranes (400–600 $\mu$mol $O_2$/mg Chl per h) were prepared from market spinach by the method of Kuwabara and Murata [36], and suspended in the buffer medium containing 0.2 M sucrose, 20 mM NaCl and 20 mM Mops-NaOH (pH 6.8), with 50 vol% glycerol added. The membranes, with 6 mg Chl/ml, were stored at 77 K until use.

The membranes were transferred into Suprasil quartz tubes with inner diameter of 3 mm for CW EPR and 4 mm for pulsed EPR and incubated on ice in the dark for 2 h. The sample length in quartz tubes was about 10 mm. Thereafter the samples were illuminated for 5 min at 195 K in a methanol/solid $CO_2$ bath by 500 W tungsten-halogen light through a 10 cm thick

water layer and allowed to equilibrate for 15 min at room temperature in complete darkness. This pre-illumination treatment was applied to synchronize the centers in the 100% $D^+S_1$ state [15]. These samples were illuminated again for 5 min at 195 K. One turnover occurred into the $S_2Q_A^-Fe^{2+}$ state. Then the sample was kept in complete darkness for 2 min at 253 K prepared by a salt/ice mixture to transfer the electron from the $Q_A$ to the $Q_B$ site [37]. With these treatments we could obtain the $S_2Q_AFe^{2+}$ state in PS II. The $S_1Q_A^-Fe^{2+}$ state was obtained by illumination of the pre-illuminated sample at 77 K for 15 min. Thus, we obtained four kinds of combinations of oxidation: $S_1Q_AFe^{2+}$, $S_2Q_AFe^{2+}$, $S_1Q_A^-Fe^{2+}$ and $S_2Q_A^-Fe^{2+}$ and these states were checked by EPR of Mn-multiline [38] and $Q_A^-$ at a low temperature, as shown in Fig. 1 [22,39]. The yield of Mn-multiline and $Q_A^-Fe^{2+}$ in four oxidation states are shown in Table I.

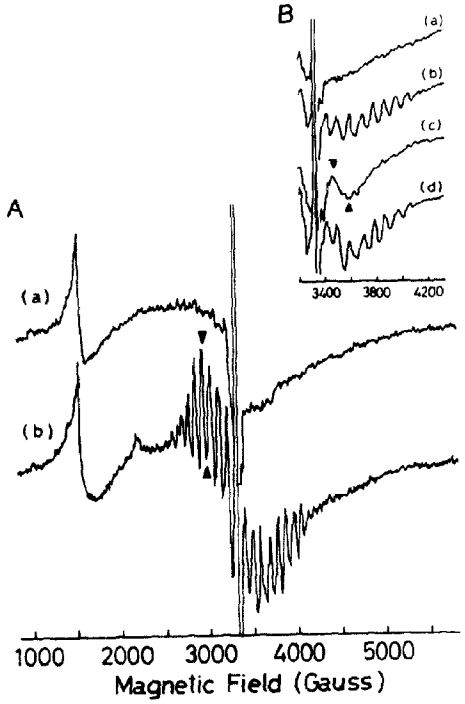


Fig. 1. (A) EPR signals in (a) $S_1Q_AFe^{2+}$ and (b) $S_2Q_AFe^{2+}$ states measured at a low microwave power (2 mW) by broad field sweep. (B) EPR signals at the upper field range of Sig. II, observed at a high microwave power (136 mW) in (a) $S_1Q_AFe^{2+}$, (b) $S_2Q_AFe^{2+}$, (c) $S_1Q_A^-Fe^{2+}$ and (d) $S_2Q_A^-Fe^{2+}$ states. Multi-line intensity was estimated at the peak intensity shown in arrowheads in A(b). $Q_A^-Fe^{2+}$ signal intensity was estimated from the difference at the field points indicated by two arrowheads in B(c), after subtraction of (a) from (c) in the $S_1$ and (b) from (d) in $S_2$ states, respectively. The estimated percentages are shown in Table I. EPR conditions: microwave frequency, 9.29 GHz; modulation frequency, 100 kHz; modulation width, 20 G; temperature, 6.5 K.

TABLE I

*Yields of Mn-multiline and $Q_A^-Fe^{2+}$ signal in four oxidation states*

Relative error is ±3% for Mn-multiline signal and ±5% for $Q_A^-Fe^{2+}$.

| State | $S_1Q_AFe^{2+}$ | $S_2Q_AFe^{2+}$ | $S_1Q_A^-Fe^{2+}$ | $S_2Q_A^-Fe^{2+}$ |
|---|---|---|---|---|
| Mn-multiline [a] | 0 | 100 | 0 | 95 |
| $Q_A^-Fe^{2+}$ [b] | 90 | 95 | 0 | 5 |

[a] Mn-multiline intensity obtained at the position indicated by arrowheads in Fig. 1A(b) by illumination at 200 K for 8 min was used as a standard.

[b] $Q_A^-Fe^{2+}$ intensity in $S_1Q_AFe^{2+}$ state prepared by illumination at 77 K for 30 min was used as a standard. Intensities were observed at the positions indicated by arrowheads in Fig. 1B(c).

*CW EPR measurement*

CW EPR measurement was carried out using a Bruker ESP300 system X-band spectrometer at temperatures between 77 K and 220 K by using a home-made nitrogen gas-flow cryostat with a temperature controller. We used a $TE_{011}$ mode cylindrical cavity with a window of 6 mm diameter for illumination by a laser flash for transient EPR and microwave power saturation above 90 K. For EPR at temperatures between 6.5 and 140 K, we used a standard rectangular cavity of $TE_{102}$ with an Oxford ESR-900 continuous flow cryostat. A $Cr^{3+}$-doped MgO, which has a g-value of 1.9800, was set inside each cavity and used as a reference to calibrate the signal intensity, the resonance field and the effective microwave power. The saturation characteristics of Tyr.D$^+$ were observed with a 100 kHz field modulation and the modulation amplitude of 2.5 G at 90 K. In measurement of Tyr.D$^+$ microwave saturation, the peak intensity at the low field side was plotted for various microwave powers. Accessory Chl$^+$ radical was observed in the sample with cytochrome *b*-559 oxidized by DDQ(2,3-dichloro-5,6-dicyano-*p*-benzoquinone) after illumination at 77 K for comparison with the transient $P680^+$ signal. This signal species has been characterized by different methods [40,41].

Transient EPR signals were measured by using a 1-MHz fast digitizer equipped in the Bruker ESP300 system. The digitizer began recording a spectrum by means of an external trigger at the time 100 $\mu$s earlier than a laser flash illumination. A Quantel Model YG580 Nd-YAG laser gave flashes with 80 mJ, 15 ns pulse at 532 nm. The microwave saturation characteristics of the $P680^+$ transient signal were observed at 90 K with 7 G field modulation width by signal accumulation. Because P680 cannot be oxidized in the presence of $Q_A^-$, we usually calibrated signal intensity according to the decreasing intensity with increasing flash numbers mentioned later and also by change in intensity of different samples.

*Pulsed EPR measurement*

Pulsed EPR signals were measured by a Bruker ESP380 pulse accessory equipped in a Bruker ESP300 system with 1-kW TWT amplifier, Model 117X, made in Applied System Engineering. A Bruker model ER4117 DHQ-N dielectric cavity available above 77 K was used. For $T_1$ measurement of Tyr.D$^+$ five $\pi/2$ pulses were given to saturate magnetization completely. After some variable interval of $t$, $(\pi/2)$–$\tau$–$(\pi)$ pulses were given to observe the Hahn echo indicating recovery of the magnetization. The separation of five $\pi/2$ pulses, $\tau_1$, is 8000 ns and $\tau$ is 160 ns. $\pi/2$ and $\pi$ pulse widths were 16 and 24 ns, respectively. The repetition time of the pulse sequence was 2 ms on all measurements. As the memory region is limited to 248 $\mu$s in the Bruker 380 system, we measured the full intensity of the Hahn echo without saturation pulse at every time and corrected the degree of its recovery after saturation. The observed values will be used to derive absolute values of $1/T_1$ of P680$^+$.

On the other hand the $T_2$ value of Tyr.D$^+$ was obtained by fitting the average of the two-pulse electron spin echo envelope modulation (ESEEM) to $M(\tau) = M_0 \exp(-\tau/T_2)$. $T_2$ of an accessory Chl$^+$ radical was obtained by subtraction of the dark signal from the two-pulse ESEEM decay of the light signal at the field of a $g$-value of 2.0028. $T_2$ of P680$^+$ was measured using the Carr-Purcell-Meiboom-Gill sequence [42] synchronized with laser flash on a LeCroy 9400A digital Oscilloscope, because the signal intensity decayed between flashes. $T_2$ was derived by the fitting of echo intensities, which are obtained after subtracting the data without laser flashes. To improve the S/N ratio, measurement of $T_2$ of P680$^+$ was carried out at 5 K using a loop-gap cavity. The widths of the $\pi/2$ and $\pi$ pulses were 24 and 40 ns, respectively, and the separation between the $\pi/2$ and $\pi$ pulse was 136 ns and that between $\pi$ pulses as 272 ns.

## Results and Discussion

*Transient EPR signal at 90 K*

Fig. 2(a) and (b) shows Sig.II$_s$ after and before CW illumination of the PS II for 15 min at 77 K with cytochrome *b*-559 chemically oxidized beforehand. Fig. 2(c) shows the subtraction (a)–(b). The subtracted signal is ascribed to the steady signal of Chl$^+$ which has a peak-to-peak width of 9.3 ± 0.2 G around $g = 2.0028$. Fig. 2(d) depicts the line shape of the P680$^+$ signal in the $S_1Q_A^-$ state of untreated PS II membranes. Each point indicates an average value of peak intensities of the P680$^+$ transient signal induced by laser flashes at a fixed magnetic field. The plotted signal at every 0.5 G separated magnetic field has a width of about 8.5 ± 0.5 G around $g = 2.0030 \pm 0.0002$, which is a little narrower than that in the accessory Chl$^+$ in Fig. 2(c).

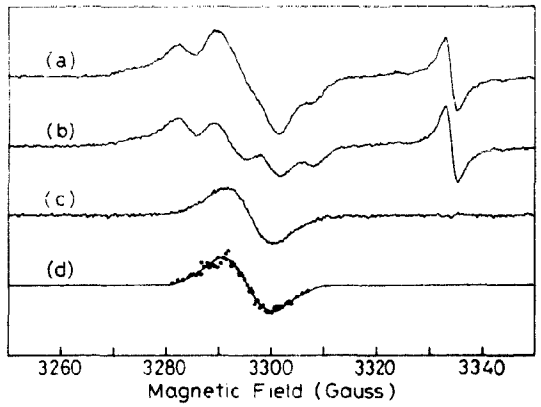


Fig. 2. EPR line shape of Chl$^+$ and P680$^+$ at 90 K. (a) Sig.II$_s$ observed in the cytochrome *b*-559 chemically oxidized PS II membranes after 15 min illumination at 77 K. (b) Sig.II$_s$ before illumination of the same sample as (a). (c) shows (a) minus (b). Chl$^+$ signal at $g = 2.0028$ with the peak-to-peak width of 9.3 G. (d) P680$^+$ transient EPR signal centered at $g = 2.0030 \pm 0.0002$, with its width 8.5 G, was obtained by the plot of averaged values over 10 accumulated peak intensities at every fixed magnetic field for untreated PS II membranes. A signal at the high-field side, $g = 1.9800$, in (a) and (b) is the $Cr^{3+}$ signal doped in MgO, which was used as a reference of $g$ values and signal intensities. EPR conditions: Microwave frequency, 9.24 GHz; modulation frequency, 100 kHz; modulation width, 2.5 G in (a) and (b), 4 G in (d); microwave power, 34 $\mu$W in (a) and (b) and 1 mW in (d).

*Temperature-dependence of decay-rate of P680$^+$*

Fig. 3 shows the Arrhenius plot of the decay rate of the flash-induced P680$^+$ EPR signal by time-resolved EPR. The characteristic decay time, $\tau$, was obtained by fitting an exponential curve to the transient signal after a laser pulse. Above 200 K the decay rate has an

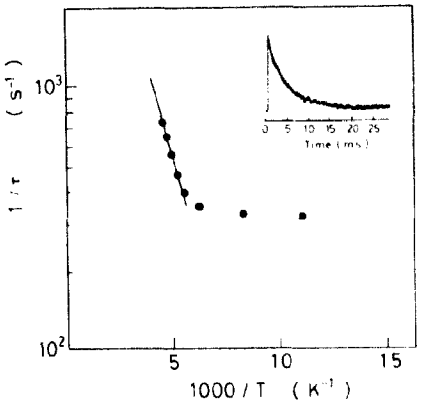


Fig. 3. Arrhenius plot of the characteristic decay rate of P680 transient signals. Above 200 K an activation energy is estimated to be 15.6 kJ/mol and below 180 K the decay rate is almost constant. Transient signals were recorded after accumulation five times above 200 K and ten times below 200 K. Inset: A transient EPR signal of P680$^+$ observed at 90 K in $S_1$ state.

activation energy of 15.6 kJ/mol. Between 180 K and 200 K the activation energy changes abruptly and below 180 K the decay rate is approximately constant. The halftime, $t_{1/2}$, is about 2 ms at 90 K. The decay time and the activation energy approximately agree with the optical spectra obtained in spinach chloroplasts by Mathis et al. [16]. Previous optical studies [16,17] have shown that the abrupt change in the activation energy can be explained by the increase in activation energy of the back reaction from $Q_A^-$. The extrapolated value to 273 K in Fig. 3 gives $t_{1/2} = 350$ $\mu$s, which is of a similar order to that given for the sample with inhibited oxygen evolution by Gerken et al. [14] and Hoganson and Babcock [25] and showing OEC did not contribute the observed signals. The observed intensity at 180 K was less than half that at 90 K, which indicates some of $P680^+$ had decayed by other recombination processes with much faster rates.

The peak intensity of the $P680^+$ transient signal decreased with increasing flash numbers at 90 K, recorded with use of a sample in the $S_2$ state. $45 \pm 5\%$ of the reaction centers of PSII were oxidized by the first laser flash, which was calibrated by the intensity of $Sig.II_s$. We observed the peak intensity increased to 70% of the reaction centers for a smaller sample size. The observed $P680^+$ was reduced by charge recombination with $Q_A^-$ by about 93%. About 7% of $P680^+$, without charge recombination, were reduced by cytochrome *b*-559 and/or Chl [16, 19]. This part of the P680 was not oxidized by the next laser flash because of the fixed negative charge on the $Q_A$ site and showed a decreasing behavior in $P680^+$ peak intensity. In fact, when all of acceptors were reduced after illumination at 77 K for 15 min or at 200 K for 5 min, the $P680^+$ transient signal could not be observed. A part of Chl nearby might be oxidized by $P680^+$ and then rereduced by cytochrome *b*-559. The electron transfer from cytochrome *b*-559 to $Chl^+$ would be a slow process [43] compared to the $P680^+$ reduction below 200 K. We could observe the transient signal of the same kinetics even in a sample with cytochrome *b*-559 chemically oxidized beforehand. We observed that neither the $Tyr.Z^+$ nor the $Chl^+$ transient signals overlapped with the observed transient signal.

Furthermore we observed a faster decreasing behavior in the peak intensity of $P680^+$ with increasing flash numbers at 180 K, compared to that at 90 K. We could not observe any $P680^+$ transient signal at all after about 15 flashes. In the sample prepared in the $S_1Q_AFe^{2+}$ state, we observed the multi-line signal after a few laser flashes above 180 K, showing that the transition from $S_1$ to $S_2$ took place after Tyr.Z had reduced $P680^+$. All these phenomena mentioned above and the value of $T_2$ shown later have proved that the transient signals observed here can be ascribed to $P680^+$.

*$T_2$ of $Tyr.D^+$ and $P680^+$*

The $T_2$ value of $Tyr.D^+$ obtained was to be about $2.7 \pm 0.2$ $\mu$s in the $S_1$ and the $S_2$ states. For $P680^+$ we

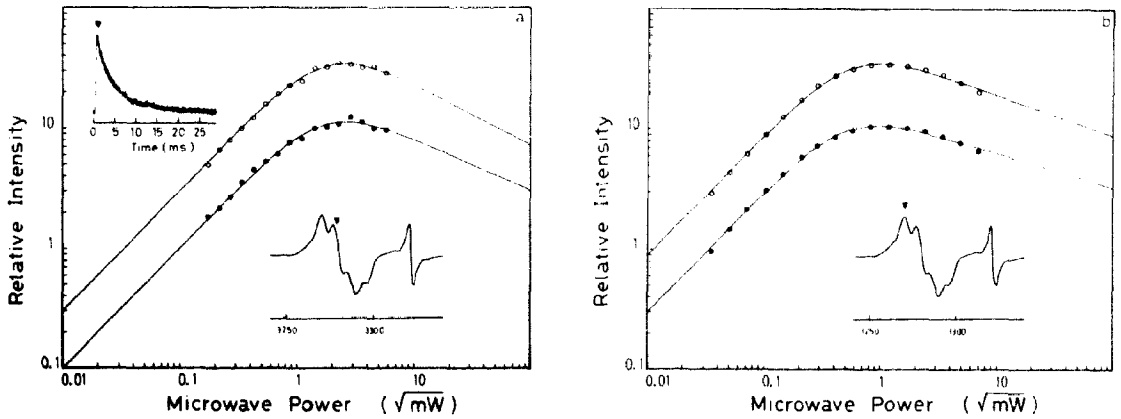


Fig. 4. (a) Microwave power saturation of $P680^+$ transient EPR signal in $S_1$ and $S_2$ states measured at 90 K. Closed and open circles show peak intensities of $P680^+$ signals at each microwave power in $S_1Q_A Fe^{2+}$ and $S_2Q_A Fe^{2+}$ states, respectively. Transient signals were recorded by 20 time accumulations at the field position of $g = 2.0058$, indicated by the arrowhead in the lower inset. Peak intensities of $P680^+$ transient signal were measured at the time shown by the arrowhead in the upper inset. The curves are a best fit with Eqn. 1. EPR conditions: microwave frequency, 9.24 GHz; modulation frequency, 100 kHz; modulation amplitude, 7 G. (b) Microwave power saturation of $Tyr.D^+$ in $S_1$ and $S_2$ states observed at 90 K with a field modulation width of 2.5 G. Other EPR conditions were the same as in (a). (●) (○) show the intensities of $Sig.II_s$ in $S_1Q_A Fe^{2+}$ and $S_2Q_A Fe^{2+}$ states, respectively at the field position shown by an arrowhead in the inset.

obtained the value of 0.9 + 0.2 $\mu$s in the $S_1$ and the $S_2$ states. We obtained the $T_2$ value 1.3 $\mu$s for the accessory Chl$^+$ oxidized by illumination at 77 K, as shown in Fig.2(c). The value of $T_2$ for P680$^+$ was comparable to that for P700$^+$ [45,46] but shorter than that for the accessory Chl$^+$. The $T_2$ of P700$^+$ in PSI, which is regarded as a chlorophyll dimer, was estimated to be about 0.5 $\mu$s [44,45]. As shown in Refs. 46 and 47, dimerization may lower the value of $T_2$. From our results of $T_2$ measurement of P680$^+$, the reaction center is considered to have a dimeric structure similar to a bacterial reaction center. Recently Mieghem et al. [48] have suggested a possibility that P680 is localized not on the special pair but on the adjacent monomeric chlorophyll based on EPR of a triplet state in oriented PS II membranes. In the triplet state the conformation of the reaction center might have been modified.

*Ratio of distances of OEC–P680 and OEC–Tyr.D*

Fig. 4 (a) and (b) show saturation characteristics of P680$^+$ and Tyr.D$^+$ measured at 90 K in two different oxidation states of the donor side. To obtain a $P_{1/2}$ value from the plotted saturation curve, we used the following equation, by taking inhomogeneous broadening into consideration [49]:

$$S \propto H_1 \frac{dI''}{dH_0} \propto \frac{P^{1/2}}{\left[1 + (P - P_{1/2})\right]^{b/2}} \qquad (1)$$

$S$ is the amplitude of a derivative signal, $P$ is an applied microwave power and $P_{1/2}$ is the microwave power at half-saturation. $b$ is an inhomogeneity parameter determined by a ratio of the Lorentzian spin packet width to the Gaussian envelope width varying from 1.0 to 3.0 for a derivative signal. From our results, $b$ was estimated to be about 1.2 for Sig.II$_s$ and about 1.8 with a more homogeneous character for the P680$^+$ EPR signal.

When the Bloch equation is applied [50], $P_{1/2}$ of the EPR signal is given by the following formula:

$$P_{1/2} \propto \frac{1}{\gamma^2 T_1 T_2} \qquad (2)$$

The relation between values of $T_1T_2$ in two different signals for Tyr.D$^+$ and P680$^+$ can be derived from Eqn. 2, as given by the following, with $\gamma$ being the same in both radicals:

$$\frac{P_{1/2}(\text{Tyr.D}^+)}{P_{1/2}(\text{P680}^+)} = \frac{T_1T_2(\text{P680}^+)}{T_1T_2(\text{Tyr.D}^+)} \qquad (3)$$

We obtained the values of $P_{1/2}$ and $T_2$ for P680$^+$ and Tyr.D$^+$ in the two definite states. To derive the absolute values of $T_1$ of four states at 90 K, the value of $T_1$ of Tyr.D$^+$ in the $S_1Q_A^-Fe^{2+}$ state was directly measured by using the saturation recovery technique of the Hahn echo signal. The $T_1$ value of 127.5 $\mu$s in the $S_1Q_A^-Fe^{2+}$ state was obtained by fitting the data with the following exponential function:

$$M(t) = M_0\{1 - \exp(-t/T_1)\} \qquad (4)$$

$t$ is an interval between the fifth saturation pulse and the $\pi/2$ pulse to obtain the Hahn echo. $M(t)$ is a Hahn echo amplitude at $t$ $\mu$s. $M_0$ is the amplitude of the Hahn echo without saturation pulses. We obtained the best fit with the single value of $T_1$, which is different from the result of two components in $T_1$ measured by Evelo et al. [32]. The difference may be ascribed to our complete saturation of magnetization by a five $\pi/2$ pulse train and/or to the difference in our measured temperature range.

Using this value of $T_1$, spin-lattice relaxation rate, $1/T_1$ of the other states, P680$^+$ in both S states and Tyr.D$^+$ in the $S_2Q_A^-Fe^{2+}$ state could be determined from the following equation:

$$\left[\frac{1}{T_1}\right]_x = \frac{(T_2P_{1/2})_x}{(P_{1/2}T_1T_2)\text{Tyr.D}^+ \text{ in } S_1} \qquad (5)$$

Here $x$ implies P680$^+$ EPR in each of two states or Tyr.D$^+$ in $S_2Q_A^-Fe^{2+}$ state. The experimental values, $P_{1/2}$, for Tyr.D$^+$ and P680$^+$ transient signals in both S states and the $1/T_1$ value, of Tyr.D$^+$ in the $S_1Q_A^-Fe^{2+}$ state at 90 K are shown in Table II together with the calculated values of $1/T_1$ by Eqn. 5.

As Evelo et al. [32] developed, $1/T_1$ induced by a paramagnetic ion is shown by the following formula [51]:

$$\frac{1}{T_1} = \frac{6}{15}S(S+1)\frac{(g\beta)^4}{R^6\hbar^2}\left[\frac{\tau_c}{1+\omega_0^2\tau_c^2} + \frac{4\tau_c}{1+4\omega_0^2\tau_c^2}\right]. \qquad (6)$$

where $\tau_c$ is a correlation time related to spin-lattice relaxation of the transition metal ion. $R$ is the distance from the metal ion to the free radical of which EPR is observed. As relaxation works additively, the relaxation rates due to the $S_2$ state can be depicted by subtraction of the value in the $S_1$ state with equivalent values in

TABLE II

*Microwave power at half-saturation, $P_{1/2}$, and spin-lattice relaxation rate $1/T_1$ of P680$^+$ and Tyr.D$^+$*

Three values of $1/T_1$ were calculated by Eqn. 5 using the value * obtained directly by pulsed EPR. The error of $1/T_1$ in calculation was within 10%.

| Oxidation state | $P_{1/2}$ (mW) | | $1/T_1$ (s$^{-1}$) | |
|---|---|---|---|---|
| | P680$^+$ | Tyr.D$^+$ | P680$^+$ | Tyr.D$^+$ |
| $S_1Q_A^-Fe^{2+}$ | 3.01 ± 0.05 | 0.253 ± 0.01 | 31000 | 7843 * |
| $S_2Q_A^-Fe^{2+}$ | 3.42 ± 0.05 | 0.329 ± 0.01 | 35340 | 10200 |

other states. Then the relative distance of two different radical species from the Mn-cluster in the $S_2$ state was obtained from Eqn. 6 by assuming that each distance, $R$, is common in all states:

$$\left[\frac{R_P}{R_D}\right]^6 = \left(\left[\{(1/T_1)\text{obs. in } S_2Q_A Fe^{2+}\} - \{(1/T_1)\text{obs. in } S_1Q_A Fe^{2+}\}\right] \text{for Tyr.D}^+\right) \times \left(\left[\{(1/T_1)\text{obs. in } S_2Q_A^- Fe^{2+}\} - \{(1/T_1)\text{obs. in } S_1Q_A Fe^{2+}\}\right] \text{for P680}^+\right)^{-1} \quad (7)$$

Here $R_D$ is the distance between the Mn-cluster and Tyr.D and $R_P$ is that between the Mn-cluster and P680. Using the $1/T_1$ values in Table II, $R_P/R_D$ is determined to be $0.91 \pm 0.03$. Thus P680 is considered to lie closer to the Mn-cluster than Tyr.D in OEC. Though the relative position of P680 to the Mn-cluster in PS II has not yet been discussed, this ratio gives a reasonable value to the proposed model systems of PS II [52,53].

In the treatment so far we assumed that the difference in the $T_1$ values in the $S_1$ and $S_2$ states have been derived at exactly the same condition, except for S states. Another important factor of this estimation is an influence of cytochrome *b*-559 on the saturation characteristics of the radical species. We measured the saturation characteristics of $Tyr.D^+$ and P680 EPR in the various oxidation states of donor and acceptor states with and without cytochrome *b*-559$^+$. Any appreciable difference in saturation characteristics of $Tyr.D^+$ and $P680^+$ EPR between the two states could not be observed under the same condition except for cytochrome *b*-559 oxidation within the limits of experimental error(data not shown). We may neglect the effect of cytochrome *b*-559 oxidation, probably because the iron center in cytochrome *b*-559 is located far enough from the radical species or the correlation time of iron may be too short or too long to contribute the relaxation of the radical species at 90 K.

*Distance between Tyr.D and OEC*

The values of relaxation rate, $1/T_1$ of $Tyr.D^+$, were precisely determined at 90 K by pulsed EPR in four combinations of oxidation states of donor and acceptor sides, $S_1Q_AFe^{2+}$, $S_2Q_AFe^{2+}$, $S_1Q_A^-Fe^{2+}$ and $S_2Q_A^-Fe^{2+}$ and are shown in Table III together with the value obtained in Tris-treated PS II. In order to discuss the absolute distance between Tyr.D, the value of the correlation time $\tau_c$ should be estimated in Eqn. 6.

Fig. 5 shows the temperature dependence of saturation characteristics given by $P_{1/2}$ in $S_1Q_AFe^{2+}$ and $S_2Q_AFe^{2+}$ states with a temperature range of 10 K to 140 K. The maximum contribution was observed at about 90 K where the correlation time $\tau_c$ is about $10^{-11}$ s, as $\omega_0$ is given by $2\pi \cdot 9.5 \cdot 10^9$ s$^{-1}$. The distance between the radical species and the metal ion can be estimated, putting the value of correlation time, $S = 1/2$ for the resultant spin of the Mn(III)-Mn(IV) complex in the $S_2$ state [38] and the derived relaxation rate at the temperature into Eqn. 6. If the $S_1$ state is considered to be a diamagnetic state as shown in [32], the difference between the $S_2$ and $S_1$ state $\Delta(1/T_1) = \{(1/T_1)_{obs.S2} - (1/T_1)_{obs.S1}\} = 2100 \pm 300$ s$^{-1}$ at 90 K, the average value of $\Delta(1/T_1)$ in both fixed $Q_A$ and $Q_A^-$ states given in Table III, can be put into Eqn. 6. Taking the correlation time, $10^{-11}$, we obtain a maximum value of 27.4 Å for the distance.

The report by Dexheimer et al. [54] has shown that the $S_1$ state has an integral spin, and then the $S_1$ state may affect the relaxation rate of radical species. If we take the value for Tris-treated PS II as an intrinsic relaxation rate of $Tyr.D^+$, the difference between the $S_2$ state and this value $\Delta(1/T_1) = 3500 \pm 300$ s$^{-1}$ combined with a correlation time $2 \cdot 10^{-11}$ with an allowed error, gives a lowest value of 23.7 Å for the distance.

TABLE III

*Spin-lattice relaxation rate $1/T_1$ s$^{-1}$ of $Tyr.D^+$ at 90 K obtained by pulsed EPR*

* $1/T_1$ value in $S_2Q_AFe^{2+}$ coincides with the calculated value in the same state shown in Table II.

| Acceptor side | Donor side | | |
|---|---|---|---|
| Oxidation state | $S_1$ | $S_2$ | Tris-treated |
| $Q_AFe^{2+}$ | 7040 ± 300 | 9090 ± 300 | 6400 ± 300 |
| $Q_AFe^{3+}$ | 7840 ± 300 | 10020 ± 300 * | |

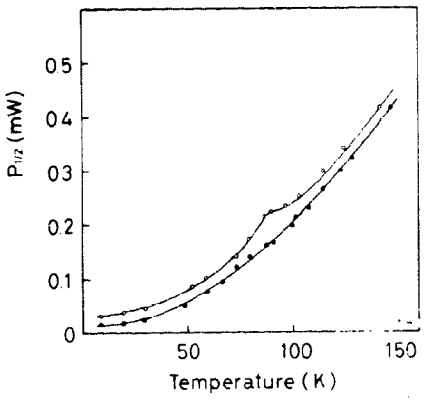


Fig. 5. Temperature-dependence of $P_{1/2}$ of Sig.II$_f$ in $S_1Q_AFe^{2+}$ state (●) and $S_2Q_AFe^{2+}$ state (○). EPR conditions were same as that in Fig. 4b, except for the cavity and the flow system. The relative error was estimated to be 10%.

Styring and Rutherford [30] observed a maximum contribution of the $S_2$ state at about 20 K, while Beck et al. [31] found a maximum in the $S_2$ state at 10 K. These maximum might be caused by other reasons, such as faster modulation frequency and magnetic field sweep [55] or other experimental conditions. The correlation time of the Mn-cluster in the $S_2$ state at 20 K can be estimated to be $10^{-9}$–$10^{-10}$, because the multiline is observable just up to this temperature. Therefore, the $S_2$ state cannot make a maximum contribution to the relaxation of Tyr.D$^+$ at this temperature.

The estimated value 23.7–27.4 Å for the distance between Tyr.D and the Mn cluster is close to the value derived by Innes et al. [33] or Isogai et al. [34] for the distance of Tyr.D from the inner membrane surface. Evelo et al. [32] suggested the distance of 28–43 Å from the maximum relaxation rate at 20 K in the $S_0$ state by assuming $S = 1/2$ to $5/2$. The range is rather wide but 28 Å seems close to our results, if they select $S = 1/2$ in the $S_0$ state.

*Supposed distance between Tyr.D and the acceptor $Q_A$*

The effect of reduction of the acceptor, $Q_A^-$, on the spin-lattice relaxation of Tyr.D$^+$ can be deduced from the values in Table III by fixing the condition of donor side at the $S_1$ or the $S_2$ state. We may try to derive the limit of distance between Tyr.D and $Q_A$ from the obtained value $850 \pm 300$ s$^{-1}$ at 90 K for $\Delta(1/T_1) = \{(1/T_1)_{obs.}$ in $Q_A^-\} - \{(1/T_1)_{obs.}$ in $Q_A\}$ given by Table III in the same way as before. Here we used $S = 1/2$ for the spin of $Q_A^-$. The value of $\tau_c$ of $Q_A^-$ may be considered to be in the same order as that of $Fe^{2+}$ because of exchange interaction between them. Norris et al. [56] observed the temperature dependence of $T_1$ of the $(BChl)_2^+$ cation radical in both natural and Fe-depleted reaction centers of the photosynthetic bacteria *Rhodopseudomonas spheroides* between 3K–200 K. They observed the maximum contribution on $1/T_1$ due to $Fe^{2+}$ at about 100 K and estimated $\tau_c$ to be nearly equal to $10^{-11}$ s at 100 K from the microwave frequency of about 9.0 GHz. We may use the result because of the similarity in structure of the acceptor side between the bacterial reaction center and PS II [53]. The correlation time of $Q_A^-$ may be estimated to be between $5 \times 10^{-12}$ and $2 \times 10^{-11}$ s with allowance of some errors at 90 K. Thus, the estimated distance between Tyr.D and $Q_A$ may fall into the region 26.5–33.3 Å. Norris et al. estimated the distance to be about 12–17 Å between $(BChl)_2$ and $Fe^{2+}$ by assuming an underestimated value of about 0.06 for $S(S+1)$ in Eqn. 6. If $S$ were taken as 2, they could obtain a reasonable value of 28 Å, close to a value of about 33 Å in a bacterial reaction center [29]. Further details of the effect of $Q_A$ reduction on Tyr.D$^+$ and other radical species are being examined.

*Distances from P680 to Mn-cluster and $Q_A Fe^{2+}$*

Based on the preceding consideration about the distance between Tyr.D and the Mn-cluster, the distance between P680 and the Mn-cluster can be deduced to be 20.8–25.8 Å from the ratio $R_P/R_D = 0.91 \pm 0.03$.

The spin-lattice relaxation rate of P680$^+$ is much larger than that of Tyr.D$^+$ at 90 K. As the intrinsic relaxation may be in the same order in both P680$^+$ and Tyr.D$^+$, the relaxation rate of P680$^+$ in the $S_1Q_A^-Fe^{2+}$ state may be considered to consist mostly of the contribution of the paramagnetic spins in the acceptor side. The difference in relaxation rate between Tyr.D$^+$ and P680$^+$ in the $S_1Q_A^-Fe^{2+}$ state given from Table III, $\Delta(1/T_1) = 25000 \pm 8000$ s$^{-1}$ will give the distance of 23–27 Å between P680 and the acceptor by assuming the same correlation time $\tau_c$ used in calculations of the distance between Tyr.D and $Q_A$. Here $S = 2$ was assumed as in the bacterial reaction center [56]. We could not decide whether the relaxation time of P680$^+$ has been shortened by the reduced $Q_A^-$ or by $Fe^{2+}$ itself, because we have no means to observe the P680$^+$ transient signal in the state of $Q_A$. The obtained value is approximately that in the bacterial reaction center [29].

## Conclusion

The distance-information deduced by spin-lattice relaxation measurements in the various combinations of oxidation states of donor and acceptor sides may be summarized in Fig. 6. In the drawing, we assumed the reaction center P680, situated at the distance of 14 Å

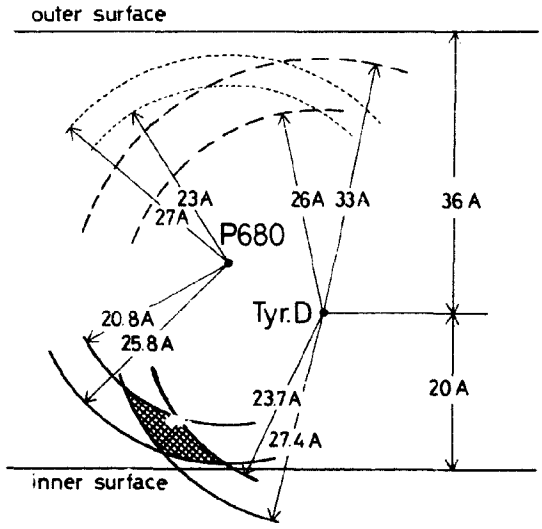


Fig. 6. Summary of relative distances in Photosystem II derived from spin-lattice relaxation time measurements of P680$^+$ and Tyr.D$^+$. The way of drawing has been mentioned in the text. The shaded area indicates the region of the Mn-cluster in OEC.

from Tyr.D, to be at the same distance from Tyr.Z, because of symmetry in D1 and D2 proteins around the reaction center, as suggested by Svensson et al. [35] and Hoganson and Babcock [25]. Two circles, with radii 23.7 and 27.4 Å, limit the distance of the Mn-cluster from Tyr.D. Then the other two circles, with radius 20.8 and 25.8 Å, limit the distance of the Mn-cluster from P680. Thus we may draw similar circles for the acceptor side to limit the position of $Q_A$ from Tyr.D and $Fe^{2+}$ from P680, though they are rather preliminary ones, derived from the data for a bacterial reaction center. The outer and inner membrane surfaces have been drawn based on the results of Isogai et al. [34]. The overlapped regions for the Mn-cluster are coincident with those presented models [52,53]. The acceptor side has a structure similar to that of the bacterial reaction center studied by X-ray [29].

## Acknowledgements

The authors are indebted to Dr. A.W. Rutherford in CEN-Saclay for discussion on the kinetics of $P680^+$ transient signal and for his critical reading of the manuscript. This work was supported by The Science Research Promotion Fund of Japan Private School Promotion Foundation and in part by Grants-in-Aid from the Ministry of Education, Science and Culture, Japan.

## References

1 Nuijs, A.M., Van Gorkom, H.J., Plijter, J.J. and Duysens, L.N.M. (1986) Biochim. Biophys. Acta 848, 167–175.
2 Wasierewski, M.R., Johnson, D.G., Seibert, M. and Govindjee. (1989) Proc. Natl. Acad. Sci. USA 86, 524–528.
3 Van Best, J.A. and Mathis, P. (1978) Biochim. Biophys. Acta 503, 178–188.
4 Schlodder, E., Brettel, K., Schatz, G. and Witt, H.T. (1984) Biochim. Biophys. Acta 765, 178–185.
5 Brettel, K., Schlodder, E. and Witt, H.T. (1984) Biochim. Biophys. Acta 766, 403–415.
6 Kok, B., Forbush, B. and Mcgloin, M., (1970) Photochem. Photobiol. 11, 456–475.
7 Saygin, Ö. and Witt, H.T. (1987) Biochim. Biophys. Acta 893, 452–469.
8 Babcock, G.T., Blankenship, R.E. and Sauer, K. (1976) FEBS Lett. 61, 286–289.
9 Dekker, J.P., Plijter, J.J., Ouwehand, L. and Van Gorkom, H.J. (1984) Biochim. Biophys. Acta 767, 176–179.
10 Renger, G. and Weiss, W. (1986) Biochim. Biophys. Acta 850, 184–196.
11 Conjeaud, H. and Mathis, P. (1980) Biochim. Biophys. Acta 590, 353–359.
12 Havemann, J. and Mathis, P. (1976) Biochim. Biophys. Acta 440, 346–355.
13 Renger, G. and Wolff, C. (1976) Biochim. Biophys. Acta 423, 610–614.
14 Gerken, S., Dekker, J.P., Schlodder, E. and Witt, H.T. (1989) Biochim. Biophys. Acta 977, 52–61.
15 Styring, S. and Rutherford, A.W. (1988) Biochim. Biophys. Acta 932, 378–387.
16 Mathis, P. and Vermeglio, A. (1974) Biochim. Biophys. Acta 368, 130–134.
17 Reinman, S. and Mathis, P. (1981) Biochim. Biophys. Acta 635, 249–258.
18 Malkin, R. and Bearden, A.J. (1975) Biochim. Biophys. Acta 396, 250–259.
19 Mathis, P., Vermeglio, A. and Haveman, J. (1976) in: Lasers in Physical Chemistry and Biophysics, pp. 465–474, Elsevier, Amsterdam.
20 Nugent, J.H.A., Evans, M.C.W. and Diner, B.A. (1982) Biochim. Biophys. Acta 682, 106–114.
21 Boska, M., Sauer, K., Buter, W. and Babcock, G.T. (1983) Biochim. Biophys. Acta 722, 327–330.
22 Nugent, J.H.A., Telfer, A. Demertriou, C. and Barber, J. (1989) FEBS Lett. 255, 53–58.
23 Ghanotakis, D.F. and Babcock, G.T. (1983) FEBS Lett. 153, 231–234.
24 Bock, C.H., Gerken, S., Stehlik, D. and Witt, H.T. (1988) FEBS Lett. 227, 141–146.
25 Hoganson, C.W. and Babcock, G.T. (1989) Biochemistry 28, 1448–1454.
26 Malkin, R. and Bearden, A.J. (1973) Proc. Nat. Acad. Sci. USA 70, 294–297.
27 Lozier, R.H. and Butler, W.L. (1974) Biochim. Biophys. Acta 333, 465–480.
28 Miller, A-F. and Brudvig, G.W. (1991) Biochim. Biophys. Acta 1056, 1–18.
29 Deisenhofer, J., Epp, O., Miki, K., Huber, R. and Michel, H. (1985) Nature (Lond) 318, 618–624.
30 Styring, S.A. and Rutherford, A.W. (1988) Biochemistry 27, 4915–4923.
31 Beck, W.F., Innes, J. B. and Brudvig, G.R. (1990) in Current Research in Photosynthesis, Vol. I, pp. 817–820, Kluwer, Dordrecht.
32 Evelo, R.G., Styring, S., Rutherford, A.W. and Hoff, A.J. (1989) Biochim. Biophys. Acta 973, 428–442.
33 Innes, J.B. and Brudvig, G.W. (1989) Biochemistry 28 1116–1125.
34 Isogai, Y., Itoh, S. and Nishimura, M. (1990) Biochim. Biophys. Acta 1017, 204–208.
35 Svensson, B., Vass, I., Cedergren, E. and Styring, S. (1991) EMBO J. 9(7), 2051–2059.
36 Kuwabara, T. and Murata, N. (1982) Plant Cell Physiol. 23 533–539.
37 Inui, T., Kawamori, A., Kuroda, G., Ono, T. and Inoue, Y. (1989) Biochim. Biophys. Acta 973, 147–152.
38 Dismukes, G.C. and Siderer, Y. (1981) Proc. Natl. Acad. Sci. USA 78, 274–278.
39 Rutherford, A.W. and Zimmermann, J.L. (1984) Biochim. Biophys. Acta 767, 168–175.
40 De Paula, J.C., Innes, J.B. and Brudvig, G.W. (1985) Biochemistry 24, 8114–8120.
41 Thompson, L.K., Miller, A.F., Buser, C.A., de Paula, J.C. and Brudvig, G.W. (1989) Biochemistry 28, 8048–8056.
42 Meiboom, S. and Gill, D. (1958) Rev. Sci. Instrum. 29, 688–691.
43 Buser, C.A., Thompson, L.K., Diner, B.A. and Brudvig, G.W. (1990) Biochemistry 29, 8977–8985.
44 Dikanov, S.A., Tsvetkov, Yu.D., Bowman, M.K. and Astashkin, A.V. (1982) Chem. Phys. Lett. 90, 149–153.
45 Dikanov, S.A., Astashkin, A.V. Tsvetkov, Yu.D. and Goldfeld, M.G. (1983) Chem. Phys. Lett. 101, 206–210.
46 Nishi, N., Schmidt, J., Hoff, A.J. and van der Waals, J.H. (1978) Chem. Phys. Lett. 56, 205–207.
47 Botter, B.J., Nonhof, C.J., Schmidt, J. and van der Waals, J.H. (1976) Chem. Phys. Lett. 43, 210–216.
48 van Mieghem, F.J.E., Satoh, K. and Rutherford, A.W. (1991) Biochim. Biophys. Acta. 1058, 379–385.

49 Rupp, H., Rao, K.K., Hall, D.O. and Commack, R. (1978) Biochim. Biophys. Acta 537, 255–269.
50 Bloch, F. (1946) Phys. Rev. 70, 460–474.
51 Solomon, I. (1955) Phys. Rev. 99, 559–565.
52 Barber, J. (1987) Trends Biochem. Sci. 12, 321–326.
53 Rutherford, A.W. (1989) Trends Biochem. Sci. 14, 227–232.
54 Dexheimer, S.L., Sauer, K. and Klein, M.P. (1990) in Current Research in Photosynthesis, Vol. I, pp. 761–764, Kluwer, Dordrecht.
55 Poole Jr., C.P. (1983) in Electron Spin Resonance, pp. 577–600, John Wiley & Sons, New York.
56 Norris, J.R., Thurnauer, M.C. and Bowman, M.K. (1980) in Advances in Biological and Medical Physics, Vol. 17, pp. 365–416, Academic Press, New York.